Research Article | Vol. 26, No. 2 | 22 Jan 2018 | OPTICS EXPRESS A54
Optics EXPRESS

Catadioptric freeform optical system design for LED off-axis road illumination applications

ZHENGBO ZHU,[1] DONGLIN MA,[1,*] QIAOMU HU,[1] YONGQIAN TANG,[1] AND RONGGUANG LIANG[2]

[1]*School of Optical and Electronic Information, Huazhong University of Science and Technology, Wuhan, Hubei 430074, China*
[2]*College of Optical Sciences, University of Arizona, 1630 E. University Blvd., Tucson, AZ 85721, USA*
**donglinma@hust.edu.cn*

Abstract: The aim of this paper is to develop a new composite structure of catadioptric optical system containing both freeform refractive surface and freeform total internal reflective (TIR) surface for LED road illumination applications. The role of freeform refractive part is to generate the shifted general rectangular illumination pattern to optimally match the shape of the road surface. The application of TIR mechanism is aimed to control the stray light in the sidewalk direction of the road luminaire and maximize the efficient energy efficiency. In this paper, we use the "double pole" ray mapping technique to design the refractive optical surface and the θ-φ coordinate ray mapping technique to derive the freeform TIR surface. The simulation shows that the novel catadioptric design has relatively high collection efficiency, thus high average illuminance level inside the effective illumination area. This lens also has good control of stray light on the backside of the road luminaire.

OCIS codes: (220.2945) Illumination design, (080.4298) Non-imaging optics, (080.4225) Nonspherical lens design, (230.3670) Light-emitting diodes.

References and links

1. G. B. Nair and S. J. Dhoble, "A perspective perception on the applications of light-emitting diodes," Luminescence **30**(8), 1167–1175 (2015).
2. N. Narendran and Y. Gu, "Life of LED-based white light sources," J. Disp. Technol. **1**(1), 167–171 (2005).
3. W. A. Parkyn, "Illumination lenses designed by extrinsic differential geometry," Proc. SPIE **3482**, 389–396 (1998).
4. H. Ries and J. Muschaweck, "Tailored freeform optical surfaces," J. Opt. Soc. Am. A **19**(3), 590–595 (2002).
5. J. Chaves, *Introduction to Nonimaging Optics* (CRC Press, 2008).
6. R. Winston, J. C. Miñano, P. Benítez, N. Shatz, and J. C. Bortz, *Nonimaging Optics* (Elsevier, 2005).
7. Z. Li, S. Yu, L. Lin, Y. Tang, X. Ding, W. Yuan, and B. Yu, "Energy feedback freeform lenses for uniform illumination of extended light source LEDs," Appl. Opt. **55**(36), 10375–10381 (2016).
8. C. Sun, X. Lee, I. Moreno, C. Lee, Y. Yu, T. Yang, and T. Chung, "Design of LED street lighting adapted for free-form roads," IEEE Photonics J. **9**(1), 8200213 (2017).
9. R. Wu, C. Y. Huang, X. Zhu, H. Cheng, and R. Liang, "Direct three-dimensional design of compact and ultra-efficient freeform lenses for extended light sources," Optica **3**, 840–843 (2016).
10. M. A. Moiseev, L. L. Doskolovich, and N. L. Kazanskiy, "Design of high-efficient freeform LED lens for illumination of elongated rectangular regions," Opt. Express **19**(Suppl 3), A225–A233 (2011).
11. Z. Feng, Y. Luo, and Y. Han, "Design of LED freeform optical system for road lighting with high luminance/illuminance ratio," Opt. Express **18**(21), 22020–22031 (2010).
12. I. Moreno, M. Avendaño-Alejo, T. Saucedo-A, and A. Bugarin, "Modeling LED street lighting," Appl. Opt. **53**(20), 4420–4430 (2014).
13. X. H. Lee, I. Moreno, and C. C. Sun, "High-performance LED street lighting using microlens arrays," Opt. Express **21**(9), 10612–10621 (2013).
14. X. Hu and K. Qian, "Optimal design of optical system for LED road lighting with high illuminance and luminance uniformity," Appl. Opt. **52**(24), 5888–5893 (2013).
15. A. Ge, J. Cai, D. Chen, H. Shu, P. Qiu, J. Wang, and L. Zhu, "Optical design of a street lamp based on dual-module chip-on-board LED arrays," Appl. Opt. **53**(25), 5750–5754 (2014).
16. S. Zalewski, "Design of optical systems for LED road luminaires," Appl. Opt. **54**(2), 163–170 (2015).
17. S. V. Kravchenko, E. V. Byzov, M. A. Moiseev, and L. L. Doskolovich, "Development of multiple-surface optical elements for road lighting," Opt. Express **25**(4), A23–A35 (2017).

#307384 https://doi.org/10.1364/OE.26.000A54
Journal © 2018 Received 18 Sep 2017; revised 3 Nov 2017; accepted 23 Nov 2017; published 4 Dec 2017

Optics EXPRESS

18. S. Wang, K. Wang, F. Chen, and S. Liu, "Design of primary optics for LED chip array in road lighting application," Opt. Express **19**(Suppl 4), A716–A724 (2011).
19. Z. Zhu, X. Yuan, R. Liang, and D. Ma, "Free-form surface generation in a double pole coordinate system for off-axis illumination application," Appl. Opt. **56**(4), 771–776 (2017).
20. D. Ma, Z. Feng, and R. Liang, "Freeform illumination lens design using composite ray mapping," Appl. Opt. **54**(3), 498–503 (2015).
21. D. Ma, Z. Feng, and R. Liang, "Tailoring freeform illumination optics in a double-pole coordinate system," Appl. Opt. **54**(9), 2395–2399 (2015).
22. City of Los Angeles Department of Public Works, "Design Standards and Guidelines", 2007–03.
23. D. Ma, S. Pacheco, C. Wang, and R. Liang, "Freeform optics construction with nonuniformly sampled grids in modified double-pole coordinate system," Opt. Eng. **54**(12), 125102 (2015).
24. F. R. Fournier, W. J. Cassarly, and J. P. Rolland, "Fast freeform reflector generation usingsource-target maps," Opt. Express **18**(5), 5295–5304 (2010).
25. R. Zhu, Q. Hong, H. Zhang, and S. T. Wu, "Freeform reflectors for architectural lighting," Opt. Express **23**(25), 31828–31837 (2015).
26. G. Yu, S. Ding, J. Ji, and T. Guo, "A Free-form Total Internal Reflection (TIR) Lens for Illumination," Proc. SPIE **8321**, 832110 (2016).
27. Z. Zhenrong, H. Xiang, and L. Xu, "Freeform surface lens for LED uniform illumination," Appl. Opt. **48**(35), 6627–6634 (2009).
28. L. Piegl and W. Tiller, *The NURBS Book*, 2nd ed. (Springer-Verlag, 1997).
29. http://www.cree.com

1. Introduction

With emerging development of light emitting diode (LED) technologies, LEDs have been revolutionizing almost every aspect of modern life due to their incomparable advantages over traditional light sources, such as long life-time, high energy efficacy, friendliness to environment, good color rendering, and so on [1–6]. Undoubtedly there exist increasing needs for LED lighting in the field of road illumination. However, the factor that the intensity distribution of LEDs follows the Lambertian property limits their applications in our daily life including the road illumination, which generally requires an off-axis rectangular pattern to match the physical shape of road surface. To solve the issue, many researchers have proposed various ways to design the freeform optics to redistribute the intensity of LEDs to satisfy the actual application requirements [7–10]. However, those freeform lens systems are typically designed for the case where the LEDs are located right above the center of road surface, which is not always true in real applications. Figure 1 shows a typical type of road illumination system where the illumination pattern should be shifted to cover the whole road surface uniformly. Luo et al focused on achieving a uniform distribution of luminance onto the road surface, where irradiance distribution was not considered, and little discussion was provided for the final illumination pattern and the stray light control in sidewalk direction [11]. Some other researchers used tilted whole lens system and the light source to realize the shifted illumination pattern onto the road surface [12–18]. The discontinuous optical surfaces are often used in these designs to control the ray direction, potentially leading to glare. The manufacturability and higher manufacturing cost is an issue in these designs. Some research considers the off-axis illumination pattern requirement for road illumination application, but the performance is poor with regards to the uniformity and collection efficiency [11, 18].

In our previous paper, we explored a new way to design the freeform optical surface for the off-axis rectangular illumination, which can be applied to road illumination directly. However, this single freeform lens design can lead to some energy waste to the backside of the road luminaire as shown in Fig. 1 [19]. To solve the issue, in this paper we propose a catadioptric optical lens by combining freeform refractive surface and TIR surface together to generate a required irradiance distribution for road illumination. We apply our previously proposed "double pole" ray mapping technique to design the freeform surface for generating the shifted rectangular pattern. This method can provide the best topological match between the sampled source grids and the prescribed rectangular target grids as demonstrated in our previous papers [20, 21]. The Cartesian ray mapping technique is applied to design the TIR surface, redirecting stray light from the sidewalk direction to the road surface. Since the

Optics EXPRESS

pattern generated by the TIR surface cannot cover the whole road, we still need the feedback modification algorithms to redesign the freeform refractive surface to homogenize the irradiance distribution on the road surface for further improvement. This complicated catadioptric lens will not only satisfy illumination performance on the road surface, but also control the unwanted illumination pattern (as shown in Fig. 1) in the sidewalk direction to a very low level. According to our simulation result, the collection light efficiency for the prescribed target can be as high as 86.7%.

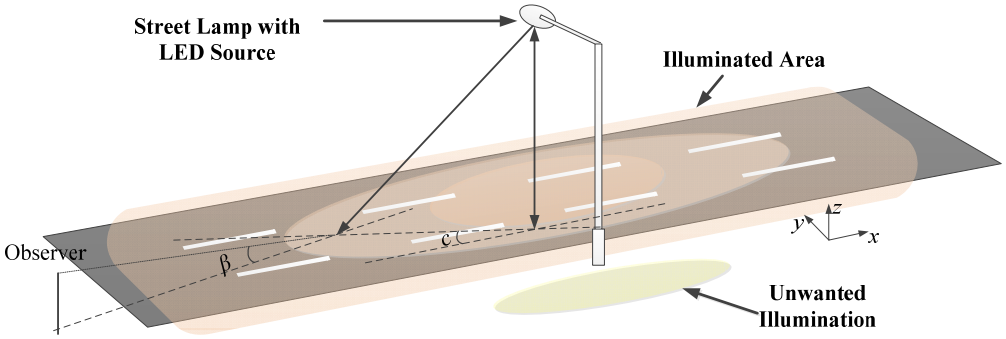

Fig. 1. Illustration of road lighting system.

2. Performance requirements and street luminaire configuration

The illumination society has laid out the standard of performance for street lighting. Table 1 lists the minimum requirements for the street luminaire in different occasions [22]. The average illuminance determines the total energy collection efficiency inside the effective illumination area. The uniformity evaluates the illumination performance of street luminaires for observers. In this paper, the method to control the unwanted illumination rays or stray light on the backside of road luminaire will be discussed. We are also aimed to improve the average illuminance level for the effective illumination area.

Table 1. Some requirements for the street luminaire performance

Road type	Uniformity ratio E_{ave}/E_{min}	Minimum average illumination level (lux)
Expressway	3.0	12.0
Bikeway	4.0	10.0
Parking Lots	3.0	22.0
Railroad Crossing	4.0	9.0
Mid-Block Crosswalks	3.0	34.0

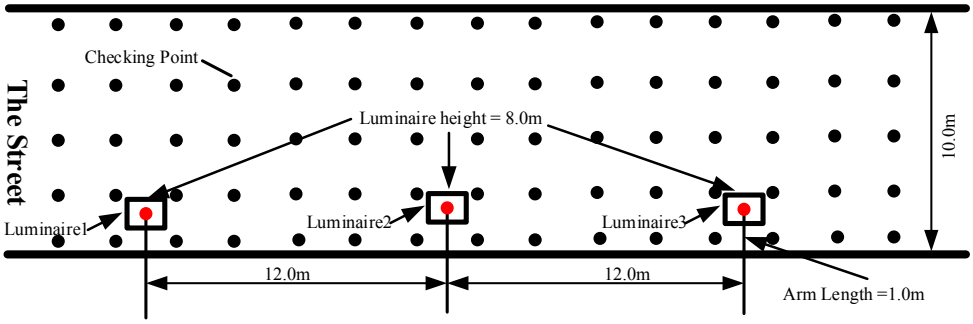

Fig. 2. The configuration of the street lighting system.

Figure 2 shows the configuration of our proposed street lighting system and the prescribed effective illumination area. For a single luminaire, the intended illumination area is defined as

Optics EXPRESS

12.0 m by 10.0 m. The mounting height of the luminaire is 8.0 m and the separation between adjacent luminaires is 12.0 m. The arm length of our designed road luminaire is set as 1.0 m.

3. Design approaches

3.1 The concept of the catadioptric lens system

The refractive lenses can generally be designed to ensure the high uniformity of the illumination on the target surface for a point-like source. However, a simple lens with only one refractive freeform surface cannot effectively redistribute the rays with large angle from LED source due to the increasing Fresnel reflection loss. However, a reflective surface can collect almost any light ray emerged from LED source, regardless its emitting angle from 0° to 90° with respect to LED normal direction. In addition, reflective optical surface can have much stronger power to deflect the light rays, very helpful in designing optics for off-axis illumination required in this road illumination. Unfortunately, pure reflective optics have the drawbacks of relatively large structure and inability to guarantee the high uniformity of prescribed illumination patterns on the target surface [23–25]. Taking these factors into consideration, total internal reflection (TIR) surface is a good candidate to collect rays with large emitting angle and provide strong deflection ability while keep a relatively compact structure. TIR surface for rotationally symmetric LED illumination has been well studied [26, 27]. A composite ray mapping algorithm has also been proposed to design a freeform TIR surface for a non-rotationally symmetric illumination [20].

In this paper, we will develop a novel method of designing a catadioptric lens composed of a freeform refractive surface and a freeform TIR surface as shown in Fig. 3 to generate an off-axis illumination pattern with high optical performance with LED located at the origin ***S***.

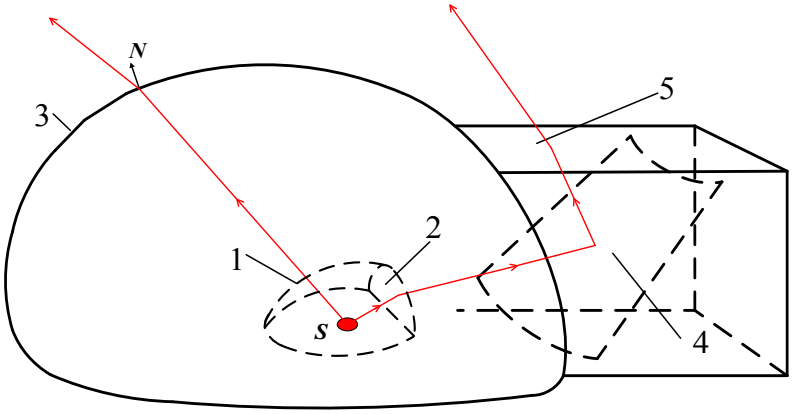

Fig. 3. Geometry of the catadioptric lens system.

As shown in Fig. 3, the catadioptric secondary optics consists of the following parts. Surface “1” is a spherical surface, collecting most of light rays from the LED source for the freeform refractive surface labeled as “3”. The center of spherical surface “1” is located below the source S. Freeform refractive surface “3” will redistribute the rays collected by surface “1” onto the whole target surface. The flat surface “2” can collect light rays towards the backside of the road luminaire and refracts these rays to the freeform TIR surface “4”. The TIR surface “4” combined with the refractive flat surface “5” can finally redistribute these rays onto the whole illumination target surface. The illumination pattern generated by the TIR channel overlaps with the pattern generated by the freeform refractive channel.

3.2 Composite ray mapping strategy for the catadioptric lens system

In lossless optical system, the energy emitted from the light source should be equal to the sum of illuminance on the target, which can be expressed as

Optics EXPRESS

$$\sum_{i=1}^{n} I(\vec{i})d\Omega_i = \sum_{j=1}^{n} E(\vec{r})dS_i, \tag{1}$$

where $I(\vec{i})$ is the luminous intensity of the LED source with a cosine distribution for a Lambertian source, $E(\vec{r})$ is the irradiance at position $\vec{r}$ on the target plane. This scheduled mapping mechanism of ray emitting direction $\vec{i}$ out of LED source and ray intersection position $\vec{r}$ with the target surface can be constructed by Snell's law and the principle of energy conservation. Figure 4 shows the mapping mechanisms for a one-to-one ray mapping and a one-to-multiple ray mapping respectively. For the one-to-one ray mapping mechanism, the illuminance level of each region on the target plane is controlled by the specific portion of the light source space. While for the one-to-multiple ray mapping (or composite ray mapping) mechanism, the illuminance level of each region on the target surface can be accumulated by source rays from two or more portions of the light source space.

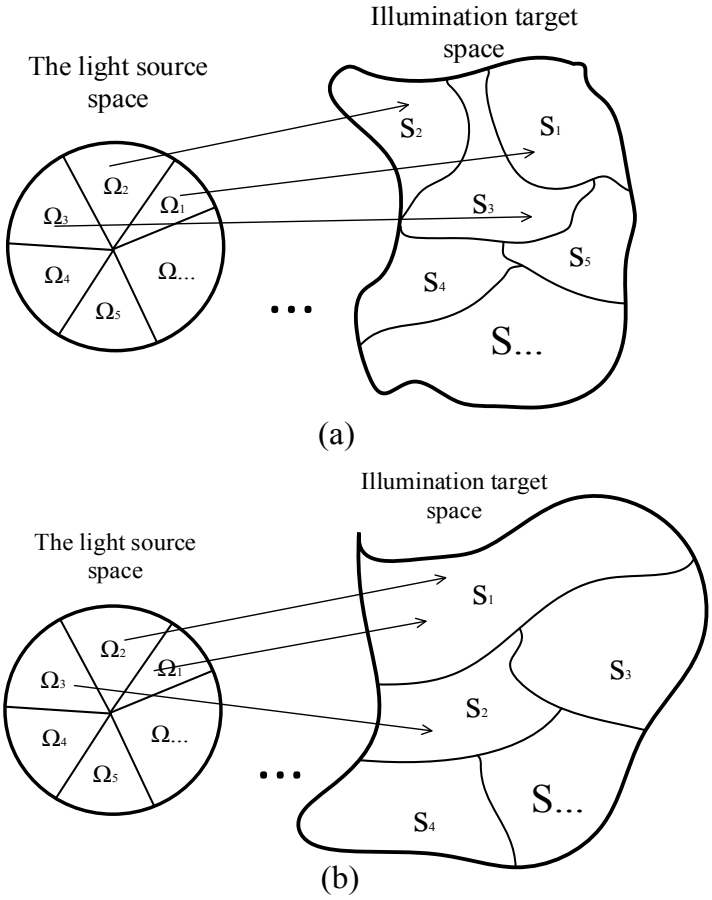

Fig. 4. General ray mapping mechanism: (a) one-to-one mapping mechanism, (b) one-to-multiple (or composite) mapping mechanism.

Optics EXPRESS

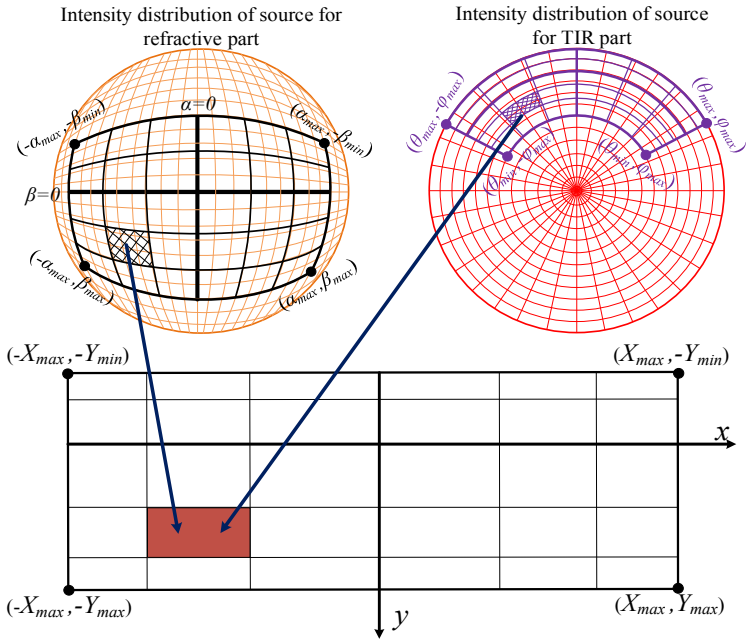

Fig. 5. Composite ray mapping mechanism between source to target.

The composite ray mapping algorithm is employed to develop the catadioptric secondary optics (Fig. 5). The emitted ray bundles of LED source are divided into two parts: one is for the refractive zone and the other one is for the TIR zone. The illuminance level of each section on the target is achieved by overlapping the rays with specific emitting direction from either zone. For the refractive part, we have introduced the double-pole coordinate system to sample the source intensity distribution and then map each source grid to the corresponding rectangular grid on the target surface. The details on this novel coordinate system as well as the corresponding source-target mapping mechanism were discussed in our previous papers [19, 21]. For the TIR surface, the (θ, φ) coordinate system is applied to sample the LED source intensity distribution for the peripheral region on back side of the road luminaire.

Using the composite ray mapping technique, we will design the freeform refractive surface and freeform TIR surface separately. The detailed derivation procedures for composite mapping relationships are provided as follows.

First, let $I_1(\alpha, \beta)$ denote the luminous intensity of the LED source and $E_1(x, y)$ be the target irradiance distribution formed by freeform refractive part of the LED source. Without energy loss, the energy conservation relationship between source and target for the refractive zone can be expressed as:

$$\iint_{\Omega_1} I_1(\alpha,\beta)\cdot\left|J(\alpha,\beta)\right|d\alpha d\beta = \iint_{D} E_1(x,y)\left|J(x,y)\right|dxdy, \tag{2}$$

where $J(\alpha, \beta)$ is the Jacobian for double pole coordinate system, $J(x, y)$ is the Jacobian for Cartesian coordinate system on the target plane. Ω_1 is the solid angle subtended by the freeform refractive collection surface, and D defines the total area of the prescribed rectangular illumination target. Ω_1 and D are defined as follows:

$$\begin{cases} \Omega_1 : \left|\alpha\right| \le \alpha_{\max};\ -\beta_{\min} \le \beta \le \beta_{\max} \\ D : \left|x_t\right| \le X_{\max};\ -Y_{\min} \le y_t \le Y_{\max} \end{cases}. \tag{3}$$

Second, we only take the LED source emission enclosed by the TIR part into consideration. Now let $I_2(\theta, \varphi)$ denote the luminous intensity of the LED source and $E_2(x, y)$ be the target irradiance distribution generated by the source rays collected by freeform TIR surface. The corresponding energy conservation relationship between source and target for the TIR zone can be expressed as:

$$\iint_{\Omega_2} I_2(\theta,\varphi)\cdot\left|J(\theta,\varphi)\right|d\theta d\varphi = \iint_{D} E_2(x,y)\cdot\left|J(x,y)\right|dxdy, \tag{4}$$

where $J(\theta, \varphi)$ is the Jacobian for the (θ, φ) coordinate system, Ω_2 is the solid angle subtended by the right-side peripheral region, it is defined as following:

$$\Omega_2 : \theta_{\min} \le \theta \le \theta_{\max};\ -\varphi_{\min} \le \varphi \le \varphi_{\max}. \tag{5}$$

Among these equations, α_{xx} (subscript "xx" represents min and max separately), β_{xx}, θ_{xx} and φ_{xx} define the edges of source region in its light source space for refractive part and TIR part respectively, as shown in Fig. 4. By integrating the variables in Eq. (2) and Eq. (4) separately, we can derive ray intersection position $\boldsymbol{T_{i,j,H}}$ on the target surface as a function of ray emitting direction $\boldsymbol{P_{i,j}}$ for both zones as follows:

$$T_{i,j,H} = f(P_{i,j}), \tag{6}$$

where $T_{i,j,H}$ is the $(i_{\text{th}}, j_{\text{th}})$ point on the target plane, the corresponding ray emitting direction is represented by $P_{i,j}(\alpha(i), \beta(j))$ or $P_{i,j}(\theta(i), \varphi(j))$, and H denotes the distance between source and target.

3.3 Construction of catadioptric optical system

A large deflection angle between the incident light ray and exit light ray at refractive surface may make the freeform surface be opposite to the draft direction with an inward concave pattern, which is not manufacturable through injection molding. By shifting the center of the spherical inner surface downward z direction, the collection surface can converge the LED light rays and decrease the incident angle at the freeform refractive surface. This creative solution has been proposed in our previous work to guarantee the manufacturability of the freeform optics [19].

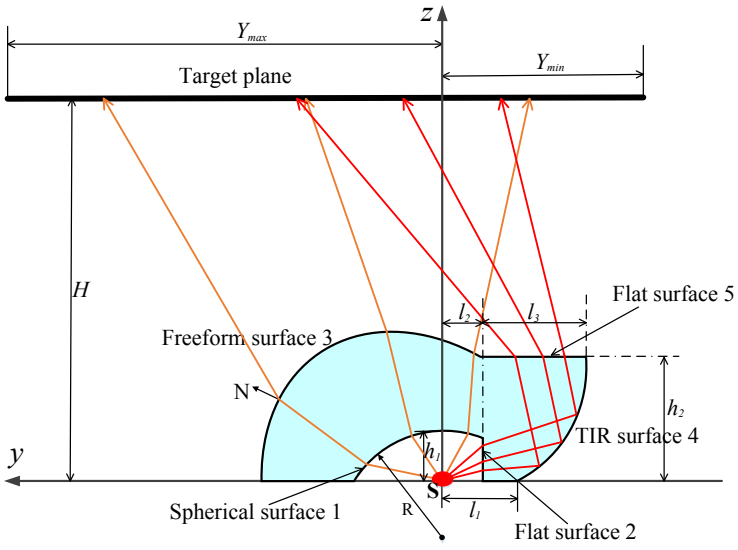

Fig. 6. The cross-section profile of catadioptric optical system.

Optics EXPRESS

Figure 6 shows the cross-section profile of catadioptric optical system with the LED source at the origin ***S***. The rays emitted from the source are divided into two parts: one part of them (the rays marked with yellow line in Fig. 6) will be redistributed by the freeform refractive optical surface, and the other portion (the rays marked as red lines) will be redirected to the target surface by the freeform TIR surface. Based on the composite ray mapping mechanism and the "double pole" ray mapping mechanism [19, 21], we can trace all emitted light rays from the LED source. As a result, for the i_{th} (i represents surface 1, 2, 3 and 5 respectively) refractive optical surface, the behavior of any specific light ray obeys the Snell's law, which can in general be expressed by:

$$\left[n_i^2 + n_o^2 - 2n_i n_o \cdot (\boldsymbol{Out}_i \cdot \boldsymbol{In}_i)\right]^{1/2} \cdot \boldsymbol{N}_i = n_o \cdot \boldsymbol{Out}_1 - n_i \cdot \boldsymbol{In}_i, \tag{7}$$

where $\boldsymbol{Out}_i$ is the normalized output vector out of the i_{th} refractive surface and $\boldsymbol{In_i}$ is the normalized incident vector into the refractive surface, n_i is the refractive index of incident space, n_o is the refractive index of output space, and $\boldsymbol{N_i}$ is the normalized normal vector at the intersection of i_{th} refractive surface. In fact, Eq. (7) can trace the ray light path inside the catadioptric lens at surface 1, 2, 3 and 5. While for the freeform TIR surface, the behavior of those incident rays follows the reflection law, which can in general be expressed by:

$$\boldsymbol{N}_4 = \frac{\boldsymbol{Out}_4 - \boldsymbol{In}_4}{\left|\boldsymbol{Out}_4 - \boldsymbol{In}_4\right|}. \tag{8}$$

Obviously, the normal vectors at surface 1, 2 and 5 are known. Output vector can be derived with Eq. (7) for a specific incident ray to both surface 1 and 2. With the calculated incident vector and corresponding output vector by mapping relationship, the normal vector at the freeform refractive surface can be achieved based on Eq. (7). While for the TIR surface "4", the situation is a little more complicate than the freeform refractive surface. We should first apply the Snell's law and Fermat's principle to specify the ray path between the TIR surface and target surface when we know the ray starting point at TIR surface and ray terminal point at the target surface with the help of mapping relationships. Then, the normal vector at each point on the TIR surface can be specified by using Eq. (8).

As a result, by tracing each single ray using the Snell's law (or reflection law) and Fermat's principle, we can find the Normal vector at any specific surface point for both the freeform refractive surface and the freeform TIR surface. With the complete information of the normal vector field for both surfaces, we can finally reconstruct the whole freeform surface by using the Newton's (or Euler's) iteration algorithm and NURBS surface fitting algorithm [28]. More detailed information about the process of constructing the freeform surface using "double pole" ray mapping technology and spherical (θ, φ) coordinate ray mapping technology have been provided in our previous papers [20, 21].

4. Design example and comparison

To demonstrate the performance of our proposed design algorithms of a catadioptric secondary optics for the off-axis rectangular illumination pattern, we design a catadioptric freeform lens system for the road illumination applications. We use PMMA as the material of the lens due to its low cost and good manufacturability, and its refractive index is about 1.493. For all designs in this paper, we choose Cree's chip-on-board (COB) LEDs XHP70 with effective emitting area of 4mm × 4mm [29].

Table 2. Parameters of the designed catadioptric lens model.

X_{max}/m	Y_{min}/m	Y_{max}/m	α_{max}/rad	β_{min}/rad	β_{max}/rad	θ_{min}/rad	θ_{max}/rad
12.0	2.0	10.0	5π/24	7π/48	5π/24	4π/15	π/2
φ_{max}/rad	H/m	h_1/mm	h_2/mm	l_1/mm	l_2/mm	l_3/mm	
13π/36	8.0	2.7	8.0	9.8	5.5	16.3	

Optics EXPRESS

Table 2 shows the prescribed parameters for the catadioptric lens: X_{max} is the half-width of the rectangular illumination pattern in x direction, Y_{min} is the size of the rectangular illumination pattern for the part in sidewalk direction, and Y_{max} is the size of the rectangular illumination pattern for street side. The meaning of these parameters as well as all other parameters is the same as what have been shown in Fig. 6. For the solid angle Ω_1 defined in the double-pole coordinate system, its edge parameters are defined as follows: α_{max} is ray's maximum acceptance angle in both positive and negative α direction, β_{min} is the ray's acceptance angle in negative β direction towards the sidewalk direction, β_{max} is the acceptance angle in positive β direction towards the street side. For the solid angle Ω_2 defined in (θ, φ) coordinate system, its edge parameters can be also defined as follows: θ_{min} is the light ray's minimum collection angle for the TIR zone, θ_{max} is the light ray's maximum acceptance angle for the TIR zone, φ_{max} is maximum acceptance angle in both positive and negative in φ direction for the TIR zone. Besides, H is the distance between the LED source and the road surface.

With the parameters listed in Table 2, the freeform refractive surface and the TIR surface can be calculated by using Matlab and then constructed with the help of CAD software. With the derived freeform refractive surface and TIR surface, the final catadioptric lens model can be built as shown in Fig. 7(c). The bottom view and top view of the lens model are shown in Figs. 7(a) and 7(e) separately. Both Figs. 7(b) and 7(d) have shown the section views along vertical direction and lateral direction respectively. To concatenate the irregular boundary of the catadioptric lens and maintain the mechanical stability for the lens model, we introduce an octagon flange at the basement of the lens model.

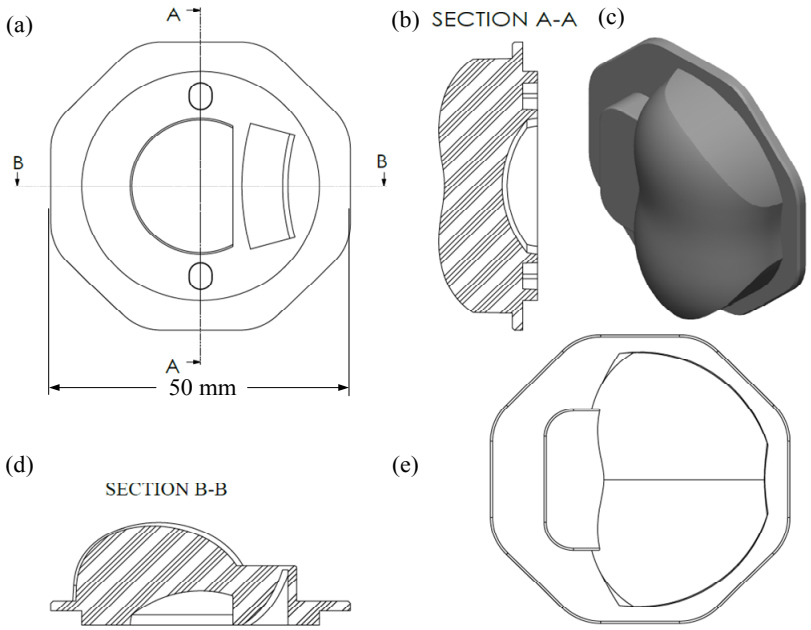

Fig. 7. Mechanical structure of the lens displayed in three views:(a) Bottom view; (b) cross-section view along vertical direction; (c) perspective view; (d) cross-section view along lateral view; (e) above view.

To demonstrate the superiority of our proposed catadioptric lens model in controlling the unwanted stray light and improving the collection efficiency inside the effective illumination area, we design another lens model with exact same design parameters but without the freeform TIR surface to generate the off-axis illumination pattern for a comparison. To verify the exact performance of our designed lens models in actual road illumination applications,

Optics EXPRESS

we align multiple luminaires for both designs along the rim of the road and check their optical performance in Lighttools. For both lens models, we trace 10 million rays to simulate their optical performance. The irradiance distribution on the target surface for our designed catadioptric lens model has been plotted in Fig. 8(a). Figure 8(b) shows the irradiance value of each analysis point on the road surface, where the contour line for iso-illuminance of each single luminaire's irradiance distribution is delineated respectively. Similarly, Fig. 9 shows the optical performance of the road luminaire systems with pure refractive optics design. We can see that both lens models have relatively good performance for the extended LED source even without any optimization or feedback modifications.

Here we use relative standard deviation (RSD), collection efficiency and average irradiance level to evaluate the general performance for road illumination applications in general. Typically, RSD is defined as:

$$RSD = \sqrt{\frac{1}{N_p}\sum_{i=1}^{N_p}\left[\frac{E_s(i)-E_0(i)}{E_0(i)}\right]^2}, \tag{9}$$

where N_p is the total number of sampling points inside effective analysis area on the target surface, $E_s(i)$ is the simulation irradiance level for i_{th} checking point on the target surface, and $E_0(i)$ is the desired illuminance requirement of the checking point on the target plane. In addition, the collection efficiency η inside the effective analysis area is defined as

$$\eta = \frac{E_{eff}}{E_{total}}, \tag{10}$$

where E_{eff} is the amount of encircled energy inside the effective analysis area on the road surface, and E_{total} is the amount of total energy on the whole road surface. Table 3 lists the quantitative comparison between the two lens models. Both designs have almost same illumination uniformity for the effective analysis area, but the catadioptric design has higher collection efficiency (measured inside the red contour) and thus higher average irradiance level (measured inside the black contour). Obviously, the special TIR structure is efficient in redirecting the stray light to the effective illumination area, improving the overall performance for the road luminaire system.

Optics EXPRESS

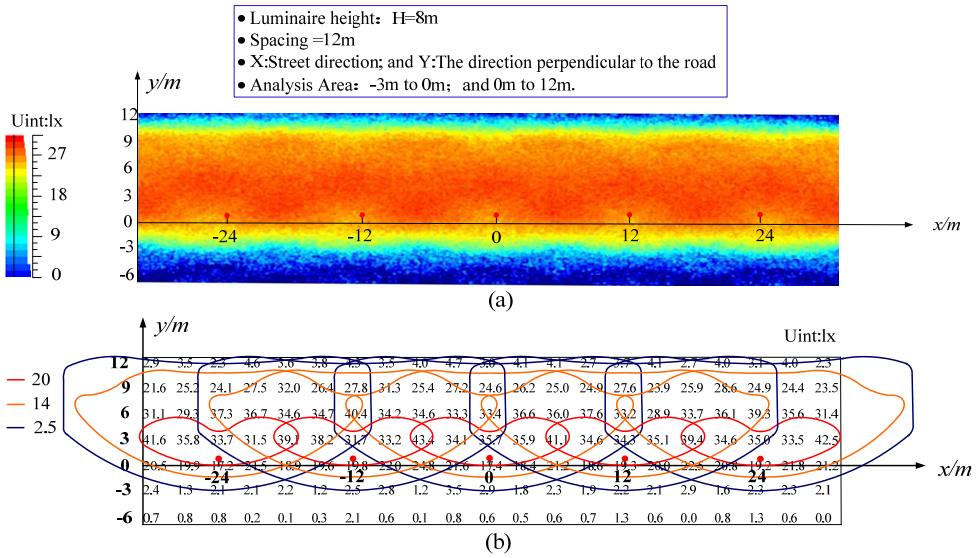

Fig. 8. Simulation results of the catadioptric optical systems: (a) irradiance distribution (b) illuminance of checking points and iso-illuminance contour of single luminaire.

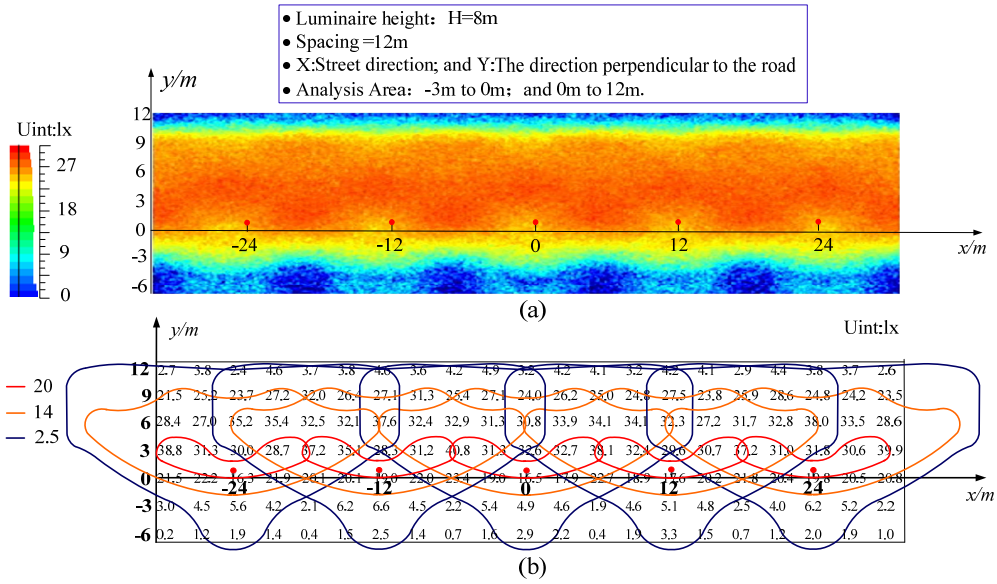

Fig. 9. Simulation results of the refractive optical systems: (a) irradiance distribution (b) illuminance of checking points and iso-illuminance contour of single luminaire.

Table 3. Overall comparison of catadioptric and refractive road luminaire systems for effective illumination area (*y*: 0-10m).

Design	*RSD*	E_{ave} (lx)	E_{min} (lx)	η	E_{ave}/E_{min}
Catadioptric optics	0.20	31	14.40	86.7%	2.15
Refractive optics	0.19	29	13.00	81.1%	2.24

The more detailed comparison results of the two designs are listed in Table 4, where the "comparison" column provides the percentage of increase in average irradiance level at

Optics EXPRESS

different locations for the catadioptric design compared to the refractive design. Obviously, catadioptric optical system with a TIR structure is a better choice to control the backward stray light and helps improve the irradiance level in effective illumination area. Table 4 quantitatively shows that the catadioptric design can have higher average irradiance level inside the effective illumination area ranging from 0m to 10m relative to the road luminaires and have much lower average irradiance level at the backside of the road luminaires.

Table 4. Comparison of refractive and catadioptric road luminaire's illumination performance.

Distance to road luminaire (m)	Average irradiance level of analysis area (lx)		
	Refractive Design	Catadioptric Design	Comparison
–3	4.36	2.14	–50.92%
0	19.74	19.88	+ 0.71%
3	32.57	35.82	+ 9.98%
6	32.30	34.49	+ 6.78%
9	25.56	25.70	+ 0.54%
0~10	29.00	31.00	+ 6.90%

5. Conclusion

In this paper, we demonstrate the feasibility of designing a catadioptric freeform optical lens by using composite ray mapping technique to generate the off-axis rectangular illumination. The novel catadioptric design is composed of a refractive part and a TIR part, and each part can realize a satisfying energy mapping between corresponding source region and the whole target surface. We have also demonstrated that the novel catadioptric design of LED secondary optics for road illumination can have superior performance on illumination uniformity, energy collection efficiency, and very good control of stray light on the backside of the road luminaire.

Funding

Wuhan Science and Technology Bureau (2017010201010110); Huazhong University of Science and Technology (2017KFYXJJ026).